Delineation of Inundated Area and Vegetation Along the Amazon Floodplain with the SIR-C Synthetic Aperture Radar

Laura L. Hess, John M. Melack, Solange Filoso, and Yong Wang

Abstract— **Floodplain inundation and vegetation along the Negro and Amazon rivers near Manaus, Brazil were accurately delineated using multi-frequency, polarimetric synthetic aperture radar (SAR) data from the April and October 1994 SIR-C missions. A decision-tree model was used to formulate rules for a supervised classification into five categories: water, clearing (pasture), aquatic macrophyte (floating meadow), nonflooded forest, and flooded forest. Classified images were produced and tested within three days of SIR-C data acquisition. Both C-band (5.7 cm) and L-band (24 cm) wavelengths were necessary to distinguish the cover types. HH polarization was most useful for distinguishing flooded from nonflooded vegetation (C-HH for macrophyte versus pasture, and L-HH for flooded versus nonflooded forest), and cross-polarized L-band data provided the best separation between woody and nonwoody vegetation. Between the April and October missions, the Amazon River level fell about 3.6 m and the portion of the study area covered by flooded forest decreased from 23% to 12%. This study demonstrates the ability of multifrequency SAR to quantify in near realtime the extent of inundation on forested floodplains, and its potential application for timely monitoring of flood events.**

I. Introduction

With space-borne synthetic aperture radar (SAR) systems, scientists studying tropical wetlands have gained a powerful research tool for understanding the ecology and hydrology of these dynamic ecosystems. Reference [1] identified the lack of information on extent and duration of flooding as a major limitation in ecological studies of rivers, and our knowledge of the floodplain hydrology of most tropical rivers has not significantly improved in the interim. The extensive seasonally flooded plains fringing large rivers modulate river flow; regulate biogeochemical processes such as generation of methane, an important greenhouse gas; serve as reservoirs of sediments and nutrients; and are critical to fisheries [2]–[5]. The extent and inaccessibility of major floodplains make remote sensing the only practical method for monitoring inundation at the basin scale. However, in tropical regions optical sensors such as the Landsat thematic mapper are severely limited by their inability to penetrate cloud cover or dense vegetation canopies.

SAR systems operating at wavelengths such as C-band (ca. 6 cm) and L-band (ca. 24 cm) are not limited by cloud cover, and detect flooding beneath many types of wetland vegetation [6]. Single-frequency SAR's have significant limitations, however: flooded herbaceous vegetation and unflooded forest may have very similar backscattering at L-band, and flooding beneath a closed forest canopy may not be detectable at C-band [7], [8]. Current SAR satellites and those planned for launch within the next two years are all single-frequency. Most work to date on tropical wetlands has been done with multi-frequency airborne systems [9], [10].

The SIR-C/X-SAR mission [11] offered the opportunity to test the ability of multi-frequency SAR to accurately map tropical floodplain inundation and vegetation from space. Here we report analysis of inundation and vegetation delineation done during the April and October 1994 SIR-C/X-SAR flights for sites on the central Amazon floodplain. Because SIR-C data for the study area were downlinked and processed during the missions, we were able to test whether such analyses could be completed very rapidly, as would be required for applications such as disaster assessment.

II. SIR-C Data and Study Site

The study area (Fig. 1) spans the floodplains of the Negro and Solimões (Amazon) rivers about 50 km west of their confluence near the city of Manaus, Brazil. SIR-C data were acquired during both Space Radar Lab (SRL) flights on datatake 46.7, a north-looking, ascending swath extending across the Amazon basin (inset, Fig. 1). Data from this swath were obtained in "realtime" mode: the radar data was transmitted to earth via TDRSS satellite within hours of acquisition, and a segment roughly centered on Barroso Island in the Solimões River was correlated by the Jet Propulsion Laboratory (JPL). For both flights, the resulting image data were electronically transmitted to the Institute for Computational Earth System Science, University of California, Santa Barbara, within 36 hours of acquisition. Datatake 46.7 was acquired in quad-pol mode (both horizontal and vertical send and receive polarizations) at C-band (5.7 cm) and L-band (24.0

Manuscript received Dec. 13, 1994; revised Apr. 28, 1995. This work was supported in part by the NASA SIR-C/X-SAR program under JPL contract 958469.

L. L. Hess is with the Institute for Computational Earth System Science, University of California, Santa Barbara, CA 93106 USA.

J. M. Melack is with the Institute for Computational Earth System Science, Santa Barbara CA 93106 USA and with the Dept. of Biological Sciences, University of California, Santa Barbara, CA 93106 USA.

S. Filoso is with the Dept. of Biological Sciences, University of California, Santa Barbara, CA 93106 USA.

Y. Wang is with the Institute for Computational Earth System Science, University of California, Santa Barbara, CA 93106 USA and with the Dept. of Geography, East Carolina University, Greenville, NC 27858 USA.

IEEE Log Number 9412808.

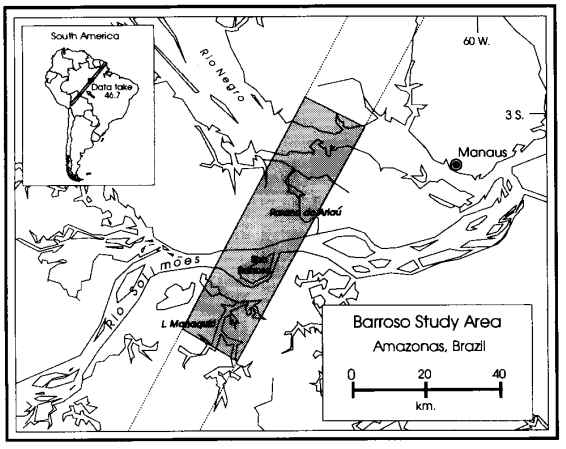

Fig. 1. Study area, showing SIR-C datatake 46.7 (inset), and segment of datatake used in this study (shaded area).

TABLE I
SIR-C DATA CHARACTERISTICS

	Space Radar Lab I	Space Radar Lab II
Datatake number	46.7	46.7
Date	12 April 1994	3 October 1994
Local time	3:07 AM	3:18 AM
Wavelengths (cm)	C-band (5.7), L-band (24.0)	C-band (5.7), L-band (24.0)
Polarizations	HH, VV, HV	HH, VV, HV
Scene center latitude,longitude	3.30°S, 60.45°W	3.24°S ,60.43°W
Incidence angle range, near-far	30.9°-34.6°	32.3°-35.6°
Number of looks	5	7
Nominal range resolution (m)	25.0	25.0
Nominal azimuth resolution (m)	25.0	25.0
Line and pixel spacing (m)	12.5	12.5

cm) wavelengths (Table I), and in VV polarization at X-band (3.0 cm); interpretation of X-band data is ongoing and is not included in this analysis. The April and October swaths were nearly exactly coincident, with similar incidence angle ranges of about 31°–35°.

The study area includes a wide variety of vegetation typical of wetlands in the central Amazon basin. The annual rise and fall of the Solimões River averages about 10 m on this reach, and inundates large areas of floodplain, known as *várzea*. Amazonian *várzea* forests have stand densities comparable to upland (*terra firme*) forests, but tend to have lower species diversity [12]. Describing a portion of *várzea* forest directly south of Barroso Island, [13] found the most important tree species to be *Pterocarpus amazonicus,* which he considered to be the most representative species for the lower Solimões *várzea*. Basal area averaged 33 m^2/ha, and the tallest trees averaged about 25 m. *Igapó* flooded forest (*sensu* [14]), also occurs in the study area, primarily in upland drainageways (*igarapés*). Less well-known wetland types within the study site include shrublands and very open woodlands occurring in low-lying areas, with clumps of trees or shrubs interspersed with open water and aquatic macrophyte beds. *Várzea* lakes and fringing shores, recent floodplain deposits, disturbed areas on levees, and the inundated forest floor all provide habitats for aquatic macrophytes, some of which have terrestrial phases [15]. Some of these species form large monospecific stands

Fig. 2. Color composites of SIR-C scenes, with CHH displayed as red, LHH as green, and LHV as blue; left, Apr. 12, 1994; right, Oct. 3, 1994.

known as floating meadows, which can have very high rates of primary productivity and of methane generation [16], [17].

III. FIELD OBSERVATIONS

The two SRL flights coincided with rising (April) and falling (October) water periods for the Solimões River. Because both floodplain inundation and vegetation phenology can change rapidly at these times, field documentation of ground conditions during the shuttle flights was critical. For both missions, conditions were documented by aerial, boat, and ground survey. In order to facilitate feedback from field team to image analysis team during the missions, potential training and test sites were identified and numbered prior to the missions based on thematic mapper and JERS-1 imagery, and flight plans for low-altitude aerial surveys were developed focusing on these sites.

Oblique hand-held video footage and 35-mm slides shot from a low-flying (500 m) aircraft documented ground conditions during the shuttle flights. Visual observations synchronized with video and slides noted presence or absence of standing water, degree of tree defoliation or macrophyte senescence, qualitative density of tree or macrophyte canopy, and presence of distinctive vegetation structures such as palms,

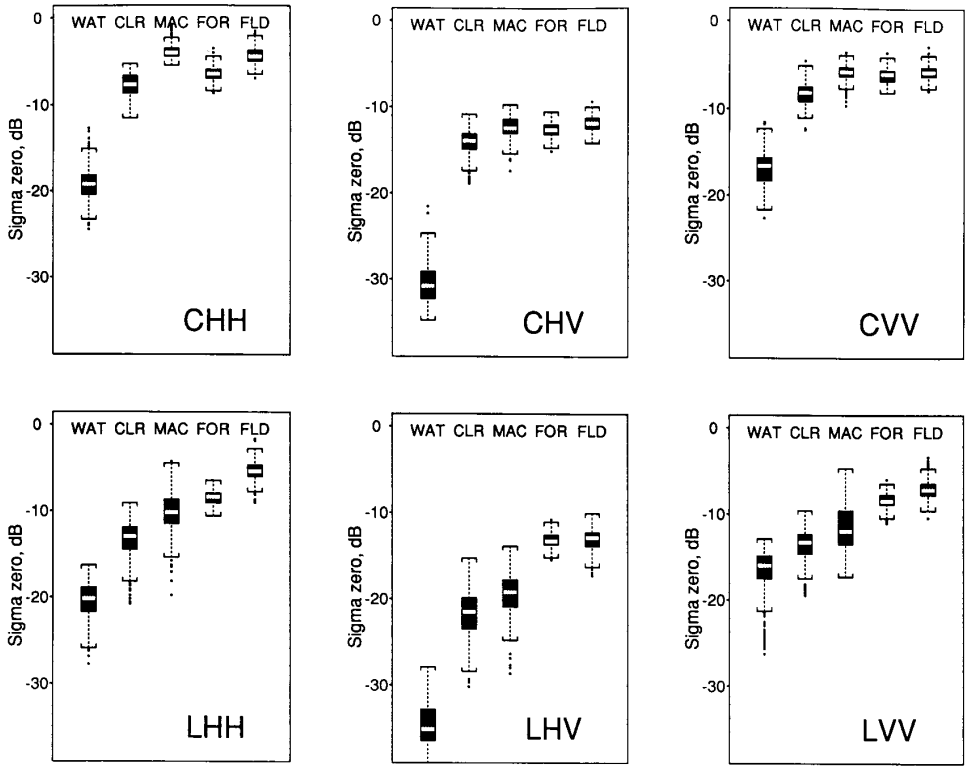

Fig. 3. Boxplots of backscattering coefficients for April training pixels, by cover type. White bar within box indicates median; upper and lower ends of box are upper and lower quartiles; dotted lines extend to nonoutliers, and outliers are plotted individually.

shrubs, plantations, or secondary growth. Visibility of sun glint, water, or soil below forest canopies allowed a determination of flooded or unflooded status for most but not all forest or shrub stands observed. Ground and boat surveys recorded the features noted above, as well as heights of macrophyte and tree canopies above water, dominant species, water depth, height to previous high-water mark, and degree of soil saturation if not flooded. Summaries of field survey data were relayed to image analyzers in Santa Barbara via telephone and fax machine. River levels were obtained from the Portobras gauge at Manaus.

IV. Image Analysis

Image analysis was carried out using the Image Processing Workbench [18], a UNIX-based public-domain image processing system within which we have implemented SAR processing software supplied by JPL. Because no external calibration devices were located within the study area, provisionally calibrated data was used for the near-realtime analyses done during the two SRL flights. Following the missions, the datatakes were reprocessed by JPL after final calibration factors were known [19]; results presented here are based on the final calibration. From the compressed format data (JPL standard multi-look product) we derived HH, VV, and HV images (which were smoothed with two iterations of a 5×5 median filter to reduce image speckle), and HH-VV phase difference (PD) images.

A pixel-based classifier classified both scenes into five vegetative-hydrologic categories: open water; flooded forest; nonflooded forest; flooded macrophyte (floating meadow); and clearing (primarily pasture or bare soil). These categories, while general, distinguish ecologically distinct units sufficient for scientific applications such as estimating areas of habitats associated with methane generation. A decision tree model was used to determine classification rules, based on training data. Decision tree classifiers (DTC's) are hierarchical multistage classifiers that can use different predictor variables at different stages of the decision process, as opposed to the globally optimal set of predictor variables used in single-stage classifiers such as parallelpiped [20]. Like neural networks, DTC's lend themselves to incremental learning as more training data become available, and usually do not depend on assumptions about the underlying distribution of the data; however, the training time for DTC's is usually much shorter, and their simple hierarchical structure greatly facilitates data interpretation compared to neural networks [20], [21]. The implementation used here is part of the S-plus statistical package [22], [23].

For each date, the eight predictor variables input to the decision tree model for each training pixel were HH, VV, and HV backscattering coefficients (dB) and |PD| (degrees) for C-band and L-band; the response variable was one of the five cover types. Based on field observations, 60 training polygons were delineated for the April scene and 55 for the October scene (from 7 to 15 per cover type); from these, 450 training

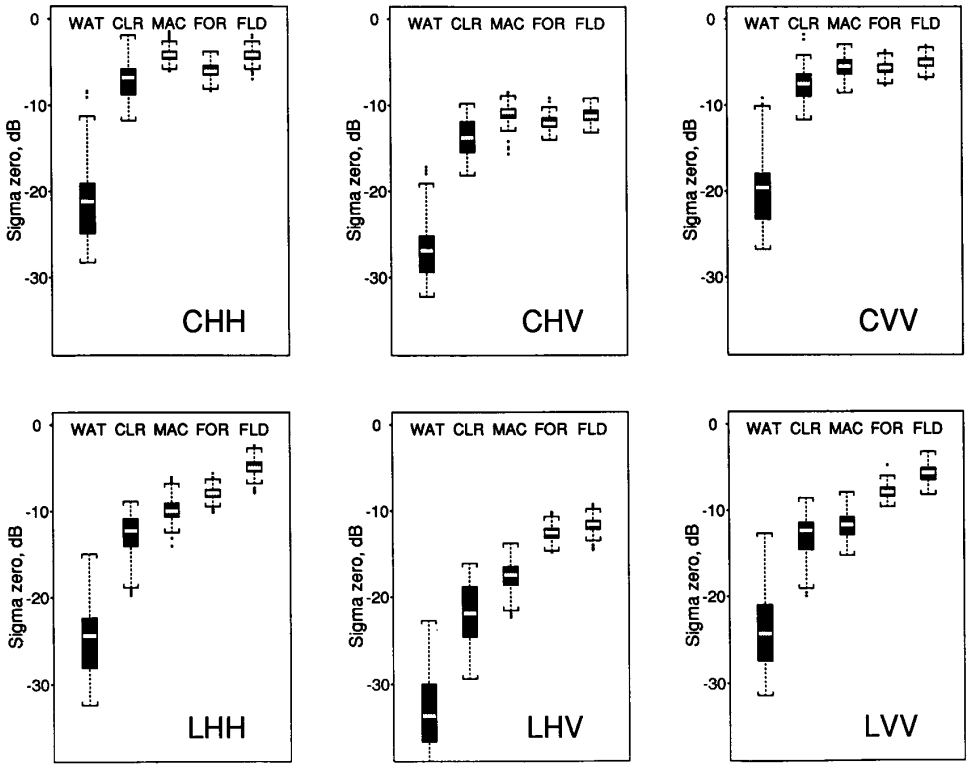

Fig. 4. Boxplots of backscattering coefficients for October training pixels.

and 450 test pixels per cover type were randomly selected. For each date, the decision tree based on the training input was "snipped" interactively until one to two terminal nodes remained for each cover type, and the resulting tree was used as the basis for classification rules. Classified images were produced within a day of receiving the data from JPL for both SIR-C flights.

V. Results and Discussion

A. General Scene Description

Color composites of the April and October SIR-C scenes are shown in Fig. 2; in these images CHH is displayed as red, LHH as green, and LHV as blue. As recorded at the Manaus gauge, the Negro River rose from 26.98 m on Apr. 12 to a peak of 29.05 m on June 26, then fell to 23.39 m on 3 October; the previous season's low-water mark (October 1993) was 19.47 m. The net decrease in river stage between April and October was thus about 3.6 m and the April and October scenes represent rising and falling water periods. The April scene was about 2 m below maximum high water and the October scene about 4 m above minimum low water. The gauge readings accord well with field observations of the previous season's high-water mark, visible on tree trunks in flooded forest stands.

A decrease in open water area (black in Fig. 2) is detectable, though not large, for some of the small lakes between the Negro and Solimões rivers, and for the large lake, Manaquiri, at the southern end of the scenes. The most obvious difference between the dates is the diminished area of flooded forest, which appears white or pale blue due to strong returns at all three bands caused by corner reflections between trunks or branches and the underlying water surface. In April, nearly all forested areas on the floodplain south of the Solimões River were inundated. The main exceptions were ridges on the floodplain west of Lake Manaquiri, and a large area of *terra firme* forest on the northeast shore of Lake Manaquiri that is not subject to inundation. By October, most of the previously flooded area south of the Solimões River has the pink and blue tone of unflooded forest, and the bright signature of flooded forests is visible only in low-lying parts of the floodplain. Flooded forest area has likewise contracted along the Parana do Ariaú (a channel linking the Negro and Solimões rivers), along upland *igarapés* near the center of the scenes, and on the peninsula on the south bank of the Negro River.

The change in conditions as water levels fall on a forested floodplain can be more complex than a transition from flooded to nonflooded forest. Tree trunks may be exposed at lower water in stands where only upper canopies were emergent at high water. Flooded forest area can increase rather than decrease as water levels fall, at sites where woody vegetation was completely submerged at high water. In October, for example, a woody shrub layer about 2.5 m above water (typically *Eugenia spruceana*) was noted at several flooded forest sites; this layer would have been submerged in April. Although there

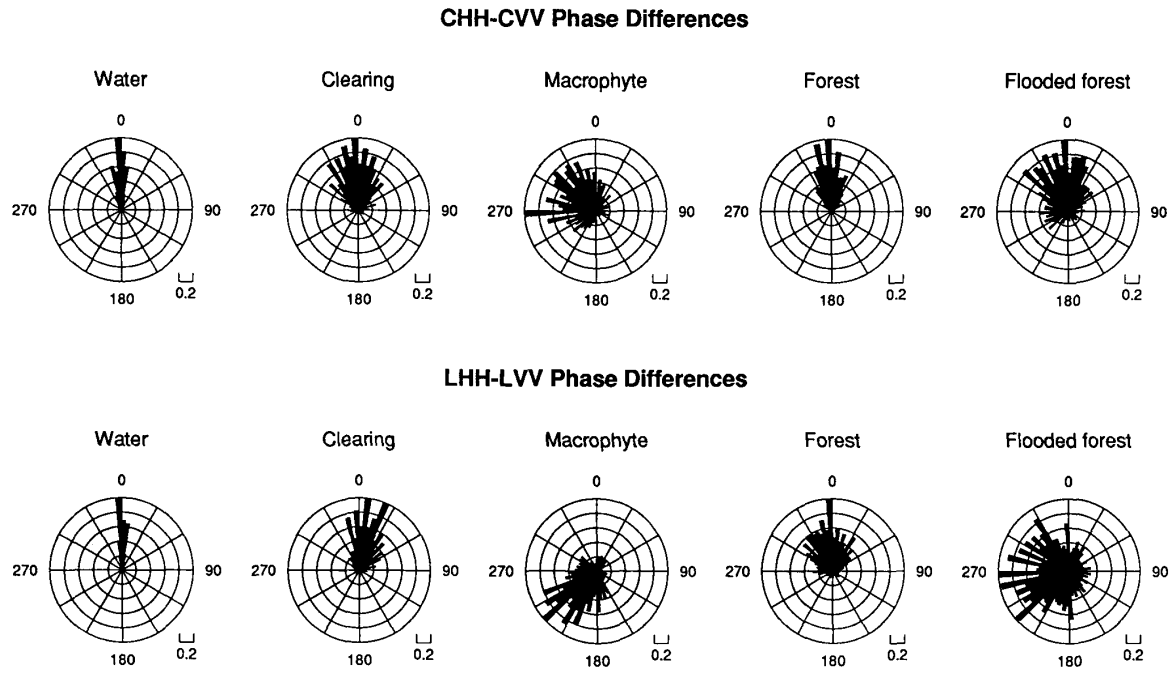

Fig. 5. Normalized polar histograms of HH-VV phase difference for April training pixels.

were differences in phenologic state for particular species, the overall extent of defoliation in flooded forests was similar for April and October. It varied by site, from stands with an insignificant amount of defoliation to those where half the trees were leafless.

Pastures and floating meadows, which scatter strongly at C-band relative to L-band, appear reddish or orange in Fig. 2. Floating macrophyte communities were found to be composed primarily of two grass species, *Echinochloa polystachya* and *Paspalum repens.* Canopy heights (80–100 cm for *Echinochloa,* 30–50 cm for *Paspalum*) were similar on both dates, and stands were dense and mostly green (although some senescent patches were visible from aerial surveys). The principal difference between high-water and low-water conditions was on the landward side of macrophyte stands, where bare soil or soil partly covered with tangles of seemingly dead grasses replaced floating meadows as floodwaters receded. Grasses commonly occurring on recently exposed ground were *Paspalum fasciculatum* and *Echinochloa polystachya*. *P. fasciculatum* is a terrestrial species that survives submergence, while *E. polystachya* has both aquatic and terrestrial growth phases [24]. While appearing senescent, stems of these grasses were still viable, and in some cases had begun to root at nodes and sprout leaves.

B. Backscattering Statistics

Statistical distributions of median-filtered σ° at CHH, CHV, CVV, LHH, LHV, and LVV polarizations for the five cover types are shown for April (Fig. 3) and October (Fig. 4). Each plotted box extends between the upper and lower quartiles of the grouped training pixels for that category, so that the box represents the middle half of the data; the bar inside the box indicates the median. Dotted lines extend to 1.5 times the interquartile range, and outliers are plotted individually. Water was clearly separable from the other categories by its low returns, particularly at C-band. CHH is the only one of the six single-frequency and polarization combinations for which clearings and macrophytes were well separated (though there is some overlap in October). Enhanced backscattering from surface water in the macrophyte stands resulted in a higher median σ° than in clearings; the difference is 3.6 dB in April and 2.6 dB in Ocober. Pastures with wet soils or ponding, which occurred on both dates though in different parts of the scene, reduced the distinction between the two categories.

On both dates, woody vegetation (forest; flooded forest or shrub) was best separated from herbaceous vegetation (clearing; macrophyte) at LHV, due to multiple scattering from branches. The difference between flooded and nonflooded forest was most pronounced at LHH (differences between medians of 2.9 dB in April and 3.0 dB in October). All flooded forest training polygons had higher median σ°_{LHH} than forest training polygons (ranging from -6.1 to -4.0 dB for flooded forest and from -9.1 to -7.3 dB for forest).

These results agree well with theoretical predictions from canopy backscatter modeling of flooded versus nonflooded forest for a tall flooded forest stand on the Negro River near the Barroso scene [25]. For that stand, with a basal area of 38 m^2/ha, the difference in backscattering between flooded and nonflooded stands was predicted to be greater at HH than at VV polarization, and greater at L-band than at C-band. At

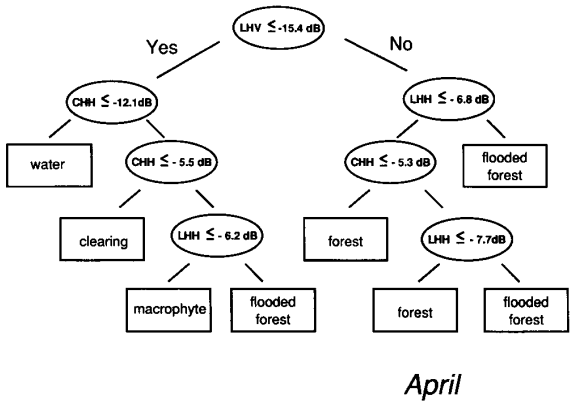

Fig. 6. Decision tree for Barroso scene, based on April training pixels.

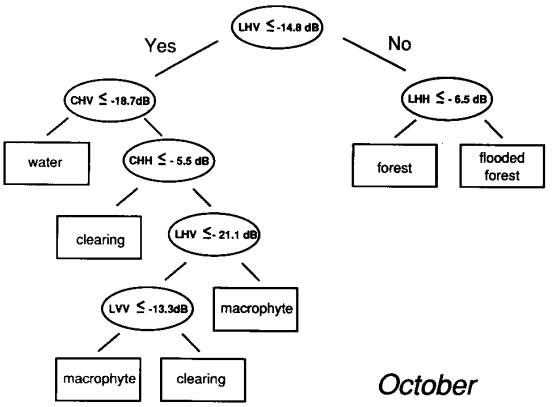

Fig. 7. Decision tree for Barroso scene, based on October training pixels.

35°, predicted σ°_{LHH} was −11 dB for nonflooded conditions and −9 dB for flooded; the difference was largely due to canopy-ground and trunk-ground scattering.

The distributions shown in Figs. 3 and 4 illustrate the difficulty of mapping these cover types using a single frequency and polarization. At LHH (the JERS-1 configuration), there is a great degree of overlap between the macrophyte and nonflooded forest categories; this confirms results of analysis of SIR-B and AIRSAR data for cypress-tupelo swamps in the southeastern United States [7], [8]. At CHH (equivalent to RADARSAT), macrophyte and flooded forest are not well separated, and at CVV (i.e., ERS-1) there is little distinction between macrophyte, forest, and flooded forest (although discrimination might be improved at ERS-1's steeper incidence angle).

Normalized histograms of HH-VV phase difference are shown in a polar format in Fig. 5 for the April training pixels (distributions for the October data were very similar). The effect of double-bounce scattering is seen for macrophytes at C- and L-bands, and for flooded forest at L-band: phase difference is offset from near 0° for clearing and forest, toward 180° for the flooded categories. The high variability of the phase difference data, which poses problems for image classification, is also evident.

C. Decision-Tree Classifier

Figs. 6 and 7 show the decision trees for April and October. Decision rules are given at each branch of the tree; e.g., for April, if σ°_{LHH} is less than or equal to −15.4 dB and σ°_{CHH} is less than or equal to −12.1 dB, the pixel is classified as water. For both dates, multifrequency information is used: CHH is used to separate water from clearings and LHH to separate flooded from nonflooded forest. CHH also separates most macrophyte from clearing pixels. In April, a subgroup of presumably larger-stemmed macrophytes are distinguished from flooded forest by lower LHH values. In October, another subgroup of macrophyte pixels is separated from clearing by lower LVV values; this is probably explained by the presence of scattered trees and shrubs in some of the pastures. Phase difference, which was found to be the most useful SAR parameter for landscape mapping of forest, wetland, and agricultural ecosystems in northern Belize [10], was not selected by the decision-tree model for either date.

TABLE II
CONFUSION MATRIX FOR APRIL TEST PIXELS

Category	Water	Clearing	Macrophyte	Non-flooded Forest	Flooded Forest	Total
Water	100.0	0	0	0	0	100
Clearing	0	98.0	1.8	0.2	0	100
Macrophyte	0	0	96.3	0.7	3.1	100
Non-flooded forest	0	0	0.2	97.5	2.3	100
Flooded forest	0	0.2	0	3.4	96.4	100

TABLE III
CONFUSION MATRIX FOR OCTOBER TEST PIXELS

Category	Water	Clearing	Macrophyte	Non-flooded Forest	Flooded Forest	Total
Water	99.3	0.7	0	0	0	100
Clearing	0	91.6	8.4	0	0	100
Macrophyte	0	1.9	96.3	1.8	0	100
Non-flooded forest	0	0.2	0	98.3	1.5	100
Flooded forest	0	0	0	4.4	95.6	100

For April, the overall misclassification rate (percent of all pixels classified into the wrong category) was 2.3% for training pixels and 2.5% for test pixels; for October the respective rates were 3.1% and 4.4%. Confusion matrices for test pixels (Tables II and III) show that misclassification rates for individual categories are less than 5% except for clearing, 8.4% of which was misclassified as macrophyte in October. Since the error rates are based on test pixels which could be unambiguously identified as a particular category, they are lower than would be expected if random pixels (which might fall somewhere between categories or might include variability not found in the training pixels) were classified and checked.

As mentioned above, one of the advantages of decision tree classifiers is that they are easily updated or augmented with new training information. The trees in Figs. 6 and 7 are optimized for their respective dates, and the decision rules vary between April and October due to both calibration uncertainty and actual scene differences in factors such as soil moisture, degree of senescence, and height of exposed canopy above water. By combining training data from multiple dates,

TABLE IV
CONFUSION MATRIX FOR COMBINED APRIL AND OCTOBER TEST PIXELS

Category	Water	Clearing	Macrophyte	Non-flooded Forest	Flooded Forest	Total
Water	100	0	0	0	0	100
Clearing	0	95.7	4.3	0	0	100
Macrophyte	0	2.7	97.1	0.2	0	100
Non-flooded forest	0	0	0	98.8	1.2	100
Flooded forest	0	0.5	2.5	7.3	89.6	100

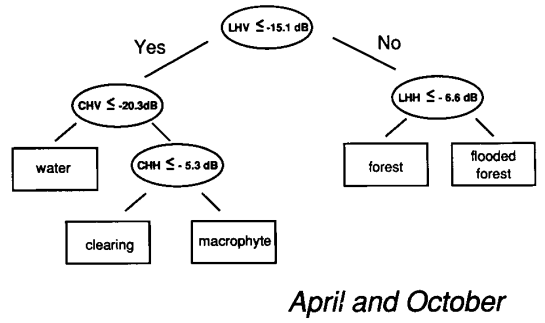

Fig. 8. Decision tree for Barroso scene, based on combined April and October training pixels.

it should be possible to accumulate a knowledge base that incorporates variability due to both calibration and seasonal change; the resulting decision rules would be less accurate for a particular scene but more robust when applied to new scenes. This possibility was tested by combining the April and October training pixels, constructing a new tree, then testing it on the combined April and October test pixels. The resulting tree (Fig. 7) closely resembles the individual April and October results, but includes only a single terminal node for each class. As expected, the overall misclassification rate for test pixels of 5.4% is higher than for the trees tailored to individual scenes, though still quite low. The highest misclassification rate is 10.4%, for flooded forest (Table IV).

Fig. 8 shows the SIR-C scenes classified using the original trees. The decrease in area of flooded forest (red) is conspicuous. Patches classified as flooded forest in the *terra firme* forest north of the Negro River are suspect, but could not be located precisely during the April aerial survey. Although seasonal flooding occurs along drainageways, some of these pixels are probably confused with flooded forest due to terrain effects. Areas on the banks of the Solimões River covered by macrophytes in April are in many cases classified as clearings in October; there are indeed many pastures and agricultural plots on the Solimões River levee that are flooded and support macrophytes at high water. Macrophyte patches appearing in clearings along roads, while they may actually be flooded herbaceous vegetation, are not equivalent to floating meadows in an ecological sense. However, due to the scene's proximity to the city of Manaus, the density of clearings is far higher than would be the case for much of the Amazon. This scene therefore probably presents a worst-case scenario for confusion of clearings and macrophytes.

Table V shows the percent coverage by land cover type for the two dates, and the change in coverage between dates.

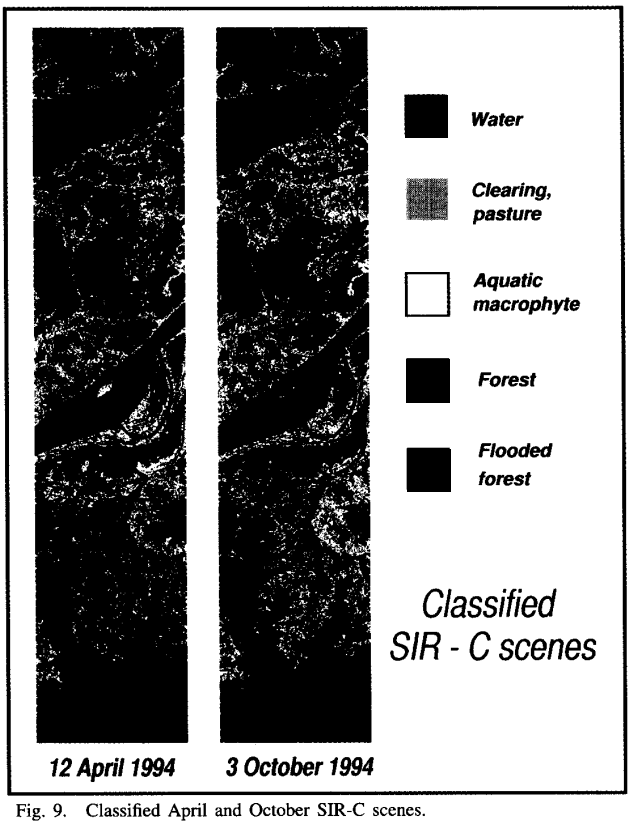

Fig. 9. Classified April and October SIR-C scenes.

TABLE V
PORTIONS OF SCENE AREAS (%) OCCUPIED BY COVER TYPES AND % CHANGE

Category	April	October	Change
Water	26.3	26.2	- 0.1
Clearing	11.9	12.2	+ 0.3
Macrophyte	5.4	4.3	- 1.1
Non-flooded forest	33.7	45.5	+ 11.8
Flooded forest	22.7	11.7	- 11.0

These figures reflect net changes for the scene, not a pixel-by-pixel comparison. The greatest changes are in area covered by nonflooded forest, which increased by 12% of the total from April to October, and flooded forest, which decreased by 11%; this represented about a 50% reduction in area of flooded forest. Other categories showed little change. The figures given in Table V apply only to this particular swath and cannot be directly extrapolated to other sections of the floodplain. Using SIR-C data acquired in wide-swath mode, this approach could be applied to larger floodplain segments.

VI. CONCLUSION

We have demonstrated that multi-frequency polarimetric SAR can accurately map flooding and vegetation on a tropical floodplain, as well as upland forest and clearings. The analysis can be completed within a few days of data acquisition, and is not subject to constraints of solar illumination or cloudiness. Backscattering statistics indicate that both C- and L-band

are necessary for accurate delineation of herbaceous versus woody and flooded vs. nonflooded cover types present at the study site. CHH provided the best separation between flooded and nonflooded herbaceous vegetation and LHH was best for flooded versus nonflooded forest, while LHV distinguished well between woody and nonwoody vegetation. Supervised classification rules can be generated very rapidly using a decision-tree model, and training data are easily incremented to include multiple dates. Although the results presented here are based on recalibrated data obtained after the missions, they are consistent with results of the original analyses carried out during the missions. We anticipate further applications of multifrequency polarimetric SAR to many ecological and biogeochemical studies of wetlands, to assessments of floods causing damage to agricultural and urban areas, and to pressing resource management needs.

ACKNOWLEDGMENT

Field work for this study was made possible by logistical and institutional support from the Instituto de Pesquisas da Amazônia (INPA), Manaus, and the Instituto Nacional de Pesquisas Espaciais (INPE), Saõ Jose dos Campos.

The authors gratefully acknowledge the assistance of B. Forsberg, W. Junk, B. Nelson, C. Padovani, and M. Piedade of INPA; D. Valeriano of INPE; J. Graae, L. Mertes, S. Miley and M. Williams of U.C. Santa Barbara; and M. Alves, B. Chapman, P. Dubois, E. O'Leary, J. Way, and A. Freeman of JPL.

REFERENCES

[1] R. L. Welcomme, *Fisheries Ecology of Floodplain Rivers.* London: Longman, 1979.

[2] K. B. Bartlett and R. C. Harriss, "Review and assessment of methane emissions from wetlands," *Chemosphere,* vol. 26, pp. 261–320, 1993.

[3] M. Goulding, *The Fishes and the Forest.* Berkeley, CA: Univ. California Press, 1980.

[4] W. J. Junk, "Ecology of swamps on the middle Amazon," in A. J. P. Gore, Ed., *Ecosystems of the World 4B. Mires: Swamp, Bog, Fen, and Moor.* Amsterdam: Elsevier, 1983.

[5] W. H. Schlesinger and J. M. Melack, "Transport of organic carbon in the world's rivers," *Tellus,* vol. 33, pp. 172–187, 1981.

[6] L. L. Hess, J. M. Melack, and D. S. Simonett, "Radar detection of flooding beneath the forest canopy: A review," *Int. J. Remote Sens.,* vol. 11, pp. 1313–1325, 1990.

[7] L. L. Hess, "L-band radar detection of standing water in forested wetlands of coastal Georgia," M.A. thesis, Univ. California, Santa Barbara, 1993.

[8] L. L. Hess, J. M. Melack, and F. W. Davis, "Mapping of floodplain inundation with multi-frequency polarimetric SAR: Use of a tree-based model," *IGARSS,* 1994, pp. 1072–1073.

[9] K. O. Pope, E. J. Sheffner, K. J. Linthicum, C. L. Bailey, T. M. Logan *et al.*, "Identification of central Kenyan Rift Valley Fever virus vector habitats with Landsat TM and evaluation of their flooding status with airborne imaging radar," *Remote Sens. Environ.,* vol. 40, pp. 185–196, 1992.

[10] K. O. Pope, J. M. Rey-Benayas, and J. F. Paris, "Radar remote sensing of forest and wetland ecosystems in the Central American tropics," *Remote Sens. Environ.,* vol. 48, pp. 205–219, 1994.

[11] E. Stofan, D. Evans, C. Schmullius, B. Holt, J. Plaut *et al.*, "Overview of results of Spaceborne Imaging Radar C, X-Band Synethetic Aperture Radar (SIR-C/X-SAR)," *IEEE Trans. Geosci. Remote Sens.,* pp. 817–828, this issue.

[12] D. G. Campbell, J. L. Stone, and A. Rosas Jr., "A comparison of the phytosociology and dynamics of three floodplain (*Várzea*) forests of known ages, Rio Juruá, western Brazilian Amazon," *Bot. J. Linn. Soc.,* vol. 108, pp. 213–237, 1992.

[13] J. D. Revilla, "Aspectos floristicos e estruturais da floresta inundavel (*várzea*) do baixo Solimões, Amazonas-Brasil." Ph.D. thesis, Instituto Nacional de Pesquisas da Amazônia and Fundaçao Universidade do Amazonas, 1991.

[14] G. T. Prance, "Notes on the vegetation of Amazonia III. The terminology of Amazonian forest types subject to inundation," *Brittonia,* vol. 31, pp. 26–38, 1979.

[15] W. J. Junk and M. T. F. Piedade, "Herbaceous plants of the Amazon floodplain near Manaus: Species diversity and adaptations to the flood pulse," *Amazoniana,* vol. 12, pp. 467–484, 1993.

[16] K. B. Bartlett, P. M. Crill, D. I. Sebacher, R. C. Harriss, J. O. Wilson, and J. M. Melack, "Methane flux from the central Amazonian floodplain," *J. Geophys. Res.,* vol. 93, pp. 1574–1582, 1988.

[17] M. T. F. Piedade, S. P. Long, and W. J. Junk, "Leaf and canopy photosynthetic CO_2 uptake of a stand of *Echinochloa polystachya* on the central Amazon floodplain," *Oecologia,* vol. 97, pp. 193–201, 1994.

[18] J. E. Frew, "The image processing workbench," Ph.D. dissertation, Univ. of Calif., Santa Barbara, 1990.

[19] A. Freeman, M. Alves, B. Chapman, J. Cruz, S. Shaffer *et al.*, "SIR-C data quality and calibration results," *IEEE Trans. Geosci. Remote Sens.,* pp. 848–857, this issue.

[20] S. R. Safavian and D. Landgrebe, "A survey of decision tree classifier methodology," *IEEE Trans. Systems Man Cybern.,* vol. 21, pp. 660–674, 1991.

[21] L. Atlas, R. Cole, Y. Muthusamy, A. Lippman, J. Connor *et al.*, "A performance comparison of trained multilayer perceptrons and trained classification trees," *Proc. IEEE,* vol. 78, pp. 1614–1619, 1990.

[22] J. M. Chambers and T. J. Hastie, *Statistical Models in S.* Pacific Grove, CA: Wadsworth and Brooks/Cole, 1992.

[23] L. A. Clark and D. Pregibon, "Tree-based models," in J. M. Chambers and T. J. Hastie, Eds., *Statistical Models in S.* Pacific Grove, CA: Wadsworth and Brooks/Cole, 1992, pp. 377–420.

[24] M. T. F. Piedade, S. P. Long, and W. J. Junk, "Biologia e ecologia de *Echinochloa polystachya* (H.B.K.) *Hitchcock* (Gramineae = Poaceae), capim semi-aquático da várzea Amazônica," *Act. Limnol. Brasil.,* vol. 6, pp. 173–185, 1993.

[25] Y. Wang, L. L. Hess, S. Filoso, and J. M. Melack, "Understanding the radar backscattering from flooded and nonflooded Amazonian forests: Results from canopy backscatter modeling," *Remote Sens. Environ.,* in press.

Laura L. Hess received the B.A. degree in soil resource management from the University of California, Berkeley, and the M.A. degree in geography from the University of California, Santa Barbara, in 1978 and 1993, respectively. She is pursuing the Ph.D. in geography at the latter university.

She is employed as a Researcher at the Institute for Computational Earth System Science, University of California, Santa Barbara. Her research interests are in applying remote sensing and GIS techniques to ecological and resource management questions, with emphases on wetlands, forests, and synthetic aperture radar.

John M. Melack received the B.A. in biological science from Cornell University, Ithaca, NY, and the Ph.D. degree from Duke University, Raleigh, NC, in 1969 and 1976, respectively.

He was an NSF Postdoctoral Fellow at the University of Michigan, Ann Arbor, and began teaching at the University of California, Santa Barbara, in 1977, where he currently is Professor of Biological Sciences and Principal Investigator in the Marine Science Institute and Institute for Computational Earth System Science. He has served on NASA's EOS Science Steering Committee and HIRIS Instrument Panel, and on National Academy of Sciences committees. He has a research program in limnology, biogeochemistry, and aquatic ecology with active studies in tropical Brazil and in California alpine and saline lakes. Synthetic aperture radar and passive microwave image analysis, and imaging spectrometry are integral part of his studies.

Solange Filoso received the B.A. degree in biological sciences from São Paulo State University, Brazil in 1985. She is pursuing the Ph.D. degree in biological sciences at the University of California, Santa Barbara.

As a Research Associate in the Institute for Computational Earth Systems Science at the University of California, Santa Barbara, since 1994, she coordinated and performed field research for the JERS-1, and SIR-C projects in the Amazon. Her research interests are the biogeochemistry of Amazon floodplains, with emphasis on forested areas, limnology, and aquatic ecology.

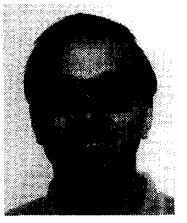

Yong Wang received the B.S. in electrical engineering and computer sciences from Northwestern Polytechnic University, China, and the Ph.D. in geography from the University of California, Santa Barbara, in 1982 and 1992, respectively.

From 1982 to 1986, he was an Electrical Engineer at Chengdu Aircraft Corp., China. From 1992 to 1994, he was a Postdoctoral Researcher at the Institute for Computational Earth System Science, University of California, Santa Barbara. In 1994, he joined the Department of Geography, East Carolina University, Greenville, NC, where he is an Assistant Professor, teaching remote sensing and geographic information system courses. His research interests are earth resources monitoring using remote sensing data, image processing and analysis technology, GIS development, and radar canopy backscattering.